Simulating the Random Dopant Effect: A New Three-Dimensional Monte Carlo Approach

Kangliang Wei, Xiaoyan Liu*, Gang Du
Institute of Microelectronics
Peking University
Beijing, China
*xyliu@ime.pku.edu.cn

Egley James
Global Foundries
Milpitas, U.S.A.

Abstract—**In this work, we present a new three-dimensional Monte Carlo (MC) method which naturally recovers the real-space carrier-impurity Coulomb interaction by mesh-based resolution of Poisson's equation. This method necessitates no additional modifications to the conventional MC simulator, thus simplifying the implementation process. The new method has been validated through the reproduction of the doping concentration dependent low-field electron and hole mobility in bulk Si. It is shown that our method can be an efficient alternative to the particle-particle-particle-mesh (P^3M) approach, which is useful for the simulation of discrete random dopant fluctuation (RDF) effect.**

Keywords-random dopant fluctuation (RDF); Monte Carlo; Coulomb interation; impurity

I. INTRODUCTION

With the continuous down scaling of the complementary metal-oxide-semiconductor (CMOS) technology, process as well as device design meets serious challenges, especially due to the increasing influence of three-dimensional (3D) effect and randomly distributed dopant fluctuation (RDF) [1, 2]. Traditionally, the method used to evaluate the effect of RDF relies on TCAD simulations [3–6], which have based themselves on the drift-diffusion or hydro-dynamic model, or the analytical compact models [7]. However, these methods tend to be inaccurate as technology enters the deca-nanometer regime, where the autocorrelation length of the microscopic random fluctuations is comparable with the feature size of devices. Hitherto there have been comprehensive 3D Monte Carlo (MC) simulations on the RDF effect [8, 9], which exploited the particle-particle-particle-mesh (P^3M) algorithm. These studies suggest that the MC method is a more reliable approach to include the RDF effect [9].

Although the P^3M method has been proved efficient, alternative approaches that can be easily implemented are still preferable. In this work we present a new 3D MC simulation method which naturally recovers the real-space carrier-impurity Coulomb interaction by mesh-based resolution of Poisson's equation. This method necessitates no additional modifications to the conventional MC simulator, which simplifies the implementation of the simulator.

II. METHODOLOGY

Instead of a continuum charge profile assumption, ionized impurities are treated discretely and randomly in our method, as is illustrated in Fig. 1. Each impurity ion is represented by a cubic grid cell of size Δ. The cube is with uniform doping concentration $N_{dop} = 1/\Delta^3$, thus the total charge of the cube to denote the unit charge that a dopant ion preserves. With this scheme, it can be reasonably assumed that the point charge of the ionized impurity can be well reproduced if Δ is small enough. To examine how Δ affects the reproduction accuracy, we performed experimental simulations, in which an electron with energy 40 meV (the thermal equilibrium energy of an electron at 300K) was to undergo a single interaction with a single impurity ion. This experimental simulation is repeated at various Δ and time step values. Fig. 2 plotted the average ratio of the electron energy change after such single carrier-impurity Coulomb interaction. It can be observed that the energy change is not sensitive to time step. This is because all the boundary crossing events in real-space have been considered in our MC simulator. However, the adoption of smaller grid size would give better energy conservation, which indicates a more precise approximation to the point charge center by the cubic grid cell.

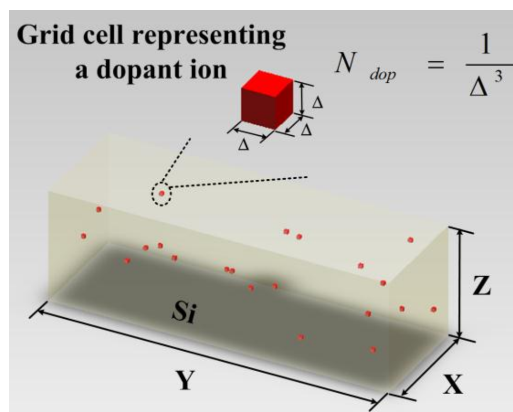

Figure 1. Dopant ions are discretely and randomly distributed in Si. Each impurity ion is represented by a grid cell of size Δ, which is with uniform doping concentration $N_{dop} = 1/\Delta^3$.

ISBN 978-0-615-71756-2

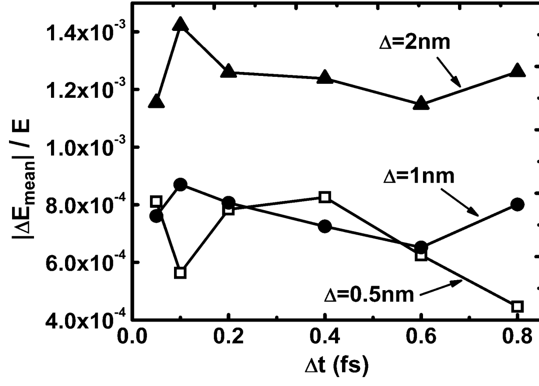

Figure 2. Average ratio of the electron energy change after single interaction with single impurity ion. Various time step Δt and mesh size Δ are considered. The initial electron energy is E=40 meV before interaction.

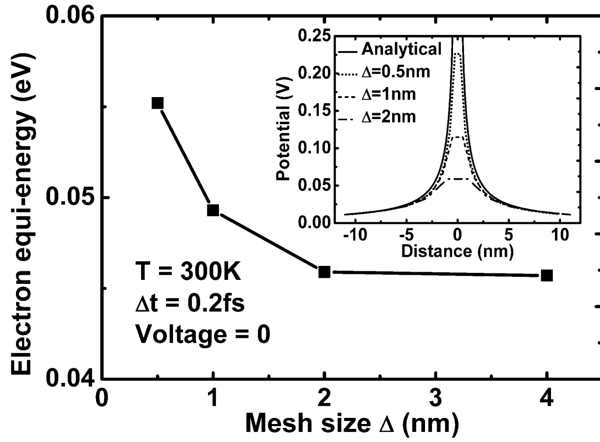

Figure 3. Influence of the mesh size Δ on the average electron equilibrium energy at 300K. Inset shows the unscreened potential profile around a single impurity ion represented by a cubic cell with various size Δ.

On the other hand, smaller grid size assumes a closer effective distance that a carrier can approach a point charge. This can be seen from the potential that an electron senses in the vicinity of a single impurity ion, as shown in the inset of Fig. 3. Nevertheless, carriers in semiconductor are charged and physically can't approach too close to a point charge center; otherwise unphysical heating of the electronic system may occur [9]. To quantify the degree of this heating effect as well as its dependence on Δ, we use different grid sizes and show the electron equilibrium energy corresponding to each Δ in Fig. 3. Clearly a lower limit for Δ must be specified. In our work, Δ ranging between 0.25–4 nm would give results well matching the experimental data.

The validation of our method is through the reproduction of the doping concentration dependent low-field electron and hole mobility in bulk Si, the results of which are shown in Fig. 4. The mobility calculated with the presented MC approach (parameters are listed in Table I) is compared with that by the conventional Brooks-Herring (BH) scattering model based on the continuous doping assumption. The former results perfectly match the experiments, while the BH model significantly overestimates the mobility, especially in the heavy doping regime. This is because the many-body interaction is well included in our approach by using the real-space resolved scattering mechanism, which is not captured in the BH model.

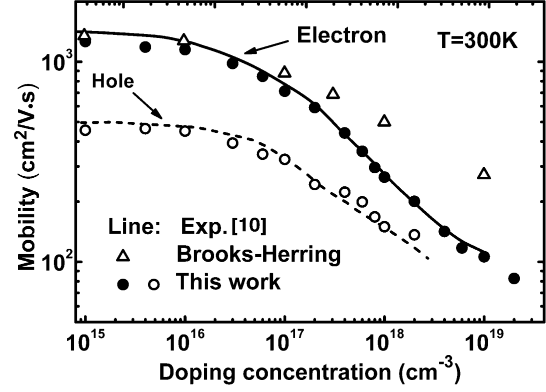

Figure 4. Low-field electron and hole mobility in bulk Si calculated with both the presented MC approach and BH scattering model. The experimental results are also shown.

TABLE I. RESISTOR PARAMETERS FOR THE DOPING RANGE OF 10^{15} — 2×10^{19} CM^{-3} USED IN THE MOBILITY CALCULATION.

Doping range (cm^{-3})	Δ (nm)	L_y (nm)	L_x/L_z (nm)
10^{15} - 10^{16}	4	400	100
10^{16} - 10^{17}	2	200	50
10^{17} - 10^{18}	1	100	20
10^{18} - 8×10^{18}	0.5	50	10
8×10^{18} - 2×10^{19}	0.25	25	4

III. RESULTS AND DISCUSSION

The capability of the proposed method to deal with the RDF effect is demonstrated in Fig. 5, which shows the simulated potential and carrier density distribution in a 100nm × 400nm × 100nm Si slab at zero electric field and with $N_D=10^{15}$ cm^{-3} (containing 4 positive impurity ions), $N_D=10^{17}$ cm^{-3} (containing 400 positive impurity ions) and $N_A=10^{17}$ cm^{-3} (containing 400 negative impurity ions), respectively. The potential and the carrier density profile fluctuation due to the discreteness and randomness of dopants are clearly captured. Note that the carriers tend to accumulate at the ion centers due to the electrostatic attraction with the ionized impurities. The accumulation of the carriers then will further reshape the potential profile around the dopant ion via the self-consistent iterative procedure between Poisson's equation and the transport. This implies the automatic inclusion of the screening effect of the ionized impurities by the free carriers in our simulator. One more advantage of this self-consistent simulation process of RDF is that another important effect in device structures with multi-material system and metal contacts —the image force—is also automatically included by solving Poisson's equation.

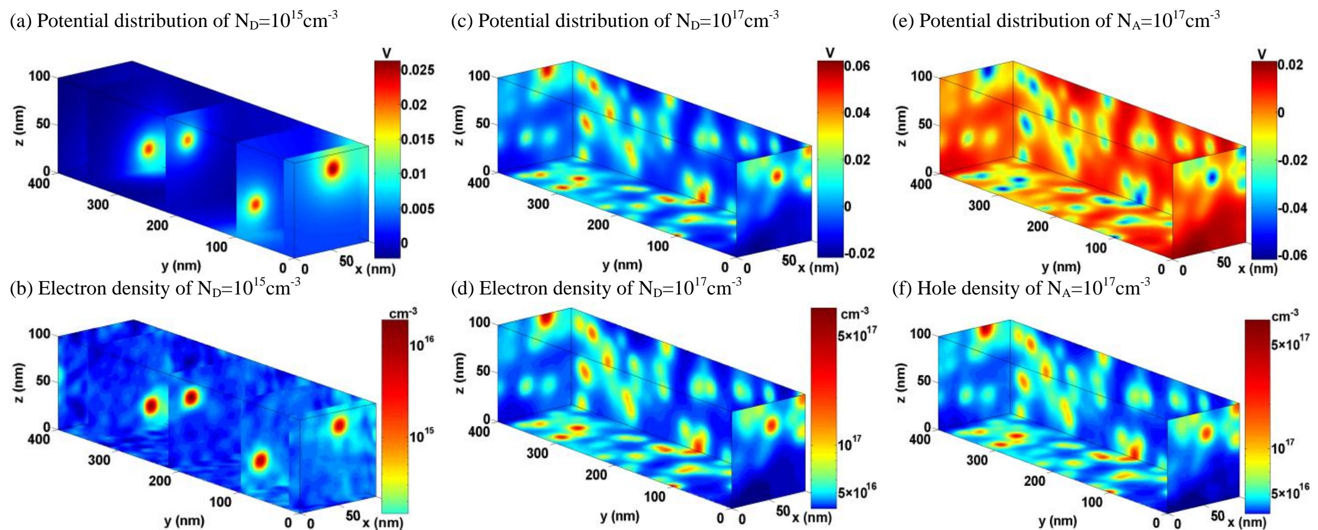

Figure 5. Simulated potential and carrier density distribution in a 100nm×400nm×100nm Si slab at zero electric field and with impurity concentration $N_D=10^{15}$ cm^{-3}, $N_D=10^{17}$ cm^{-3} and $N_A=10^{17}$ cm^{-3}, respectively.

Fig. 6 shows the impact of RDF on the drift velocity variation in a macroscopically uniformly doped Si resistor. Different nominal doping concentration of $N_D=10^{15}$ cm^{-3} and $N_D=10^{18}$ cm^{-3} is examined. We have considered both the dopant position randomness (profile #1 and #2, which have the same nominal doping concentration, but are different from each other microscopically) and number randomness (the case where one of the dopants is dropped). The experimental results for each of the doping cases are also shown for comparison [10], [11]. We can observe that velocity fluctuation is obvious at low electric field, while it is negligible at high electric field. This coincides with the regime where ionized impurity scattering mainly takes effect. Fig. 7 further shows the current susceptibility to the RDF at $N_D=10^{15}$ cm^{-3}. Both the position and number randomness of the dopants contribute to the current fluctuation. The inset of Fig. 7 shows the actual average carrier density for the same nominal doping concentration while RDF is considered. The dopant number fluctuation can influence the conduction current significantly at low doping concentrations, since only countable dopants exist. For high doping concentrations, RDF affects the conduction current mainly through the position randomness, which is shown in Fig. 8 for eight microscopically different resistor samples under $N_D=10^{18}$ cm^{-3}. The inset shows the corresponding velocity. It is noted that the maximum current fluctuation can exceed as much as 1 decade when only position randomness is considered.

Concerning the impact of RDF on non-local transport in small devices, we studied the drift velocity evolution with position for electrons injected into the sample with thermal equilibrium energy (see Fig. 8). Various nominal doping concentrations are investigated. Velocity overshoot is observed at high electric field of 10^6 V/cm. At this field, transport variation due to RDF is negligible in the overshoot region because of a much higher velocity. However, it cannot be ignored in the region where velocity saturates. The case is much different when a relatively lower electric filed (5×10^4 V/cm) is exerted on the sample. Transport variation due to RDF manifests in the whole region, especially at high nominal doping concentrations.

IV. Conclusion

In this work, we present a new 3D MC method which naturally recovers the real-space carrier-impurity Coulomb interaction by mesh-based resolution of Poisson's equation. This method necessitates no additional modifications to the conventional MC simulator, which simplifies the implementation process. The new method has been validated through the reproduction of the doping concentration dependent low-field electron and hole mobility in bulk Si. It is shown that our method can be an efficient alternative to the P^3M approach, which is useful for the simulation of RDF effect.

References

[1] W. J. Gross, D. Vasileska, and D. K. Ferry, "Ultrasmall MOSFETs: the importance of the full Coulomb interaction on device characteristics," IEEE Trans. Electron Devices, vol. 47, pp. 1831–1837, October 2000.

[2] S. Roy and A. Asenov, "Where do the dopants go?" Science, vol. 309, pp. 388–390, 2005.

[3] P. R. G. Rama, and B. Bindu, "Random dopant induced variability in SOI trigate FINFET: a simulation study," Int. Conf. on Devices, Circuits and Systems, 2012.

[4] S. Markov, B. J. Cheng, and A. Asenov, "Statistical variability in fully depleted SOI MOSFETs due to random dopant fluctuations in the source and drain extensions," IEEE Electron Device Lett., vol. 33, pp. 315–317, March 2012.

[5] G. Leung and C. O. Chui, "Variability impact of random dopant fluctuation on namoscale junctionless FinFETs," IEEE Electron Device Lett., vol. 33, pp. 767–769, June 2012.

[6] N. Sano, K. Matsuzawa, M. Mukai, and N. Nakayama, "On discrete random dopant modeling in drift-diffusion simulations: physical meaning of 'atomistic' dopants," Microelectronics Reliability, vol. 42, pp. 189–199, 2002.

[7] A. Gnudi, S. Reggiani, E. Gnani, and G. Baccarani, "Analysis of threshold voltage variability due to random dopant fluctuations in junctionless FETs," IEEE Electron Device Lett., vol. 33, pp. 336–338, March 2012.

[8] C. J. Wordelman and U. Ravaioli, "Intergration of a particle-particle-particle-mesh algorithm with the ensemble Monte Carlo method for the simulation of ultra-small semiconductor devices," IEEE Trans. Electron Devices, vol. 47, pp. 410–416, February 2000.

[9] C. Alexander, G. Roy, and A. Asenov, "Random-dopant-induced drain current variation in nano-MOSFETs: a three-dimensional self-consistent Monte Carlo simulation study using 'Ab Initio' ionized impurity scattering," IEEE Trans. Electron Devices, vol. 55, pp. 3251–3258, November 2009.

[10] Y. Taur and T. H. Ning, Fundamentals of Modern VLSI Devices, 2nd ed. Cambridge, 2009.

[11] L. Zanfi, A. Losi, C. Jacoboni, and C. Canali, "Impurity effect on high-field transport properties of electrons in silicon," IEEE Trans. Electron Devices, vol. 24, pp. 281–283, March 1977.

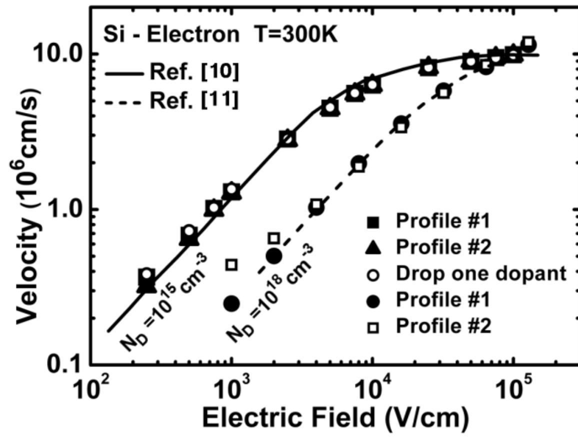

Figure 6. Electron drift velocity of $N_D=10^{15}$ cm^{-3} and $N_D=10^{18}$ cm^{-3} vs. electric field. The effects of RDF are shown.

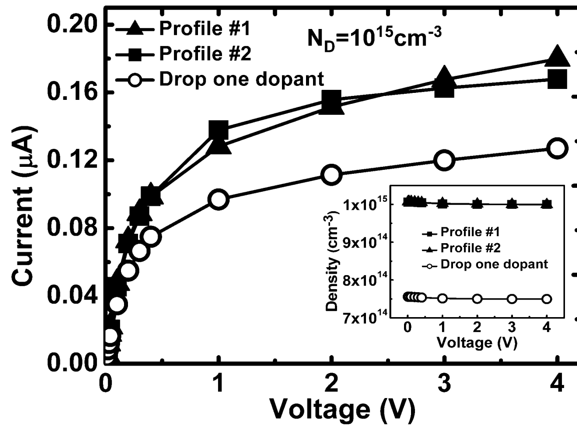

Figure 7. I-V curves of the 100nm×400nm×100nm Si slab with $N_D=10^{15}$ cm^{-3}. Both the position randomness and number randomness of dopants are considered. Inset shows the actual average carrier density for each case.

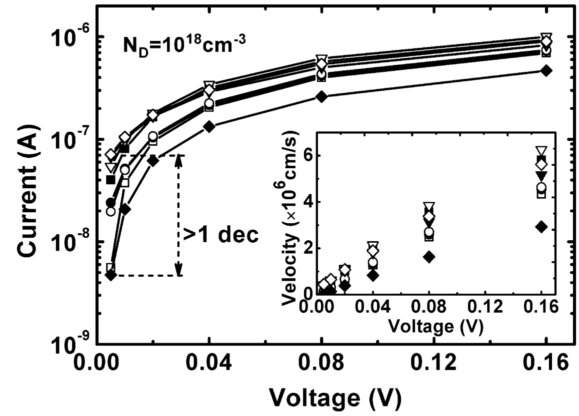

Figure 8. I-V curves of the 100nm×400nm×100nm Si slab with $N_D=10^{18}$ cm^{-3}. Only the position randomness is considered. Inset shows the corresponding velocity.

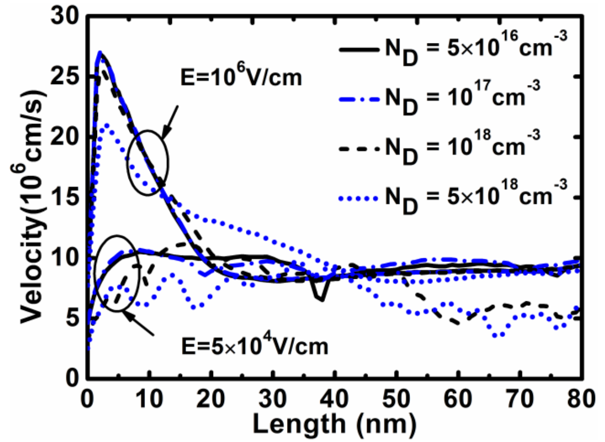

Figure 9. Electron drift velocity evolution with position for various doping concentration. Electrons injected are in the thermal equilibrium state at T=300K.